

# Rapid identification of rice seed based on inverse Fourier transform of laser-induced breakdown spectroscopy

HOU Jiaxin\* and WANG Yang'en

*College of Physics and Optoelectronic Engineering, Yangtze University, Jingzhou 434023, China*

(Received 30 August 2021; Revised 24 March 2022)

©Tianjin University of Technology 2022

The identification of rice seeds is crucial for agriculture production. An inverse Fourier transform (IFT) method based on laser-induced breakdown spectroscopy (LIBS) is proposed to identify five kinds of rice seeds. The LIBS data of the samples were preprocessed by inverse fast Fourier transform (IFFT), and the time-domain signals of rice seeds were obtained. The back propagation (BP) neural network was used to establish full spectrum, segmented spectrum, time-domain full spectrum and time-domain segmented spectrum discrimination models. Compared with the original spectrum, the time-domain spectrum can significantly improve the identification accuracy. The time-domain full-spectrum identification accuracy reached 95.28%, and the time-domain segmented spectrum identification accuracy reached 94.36%, whose identification time was only a few seconds. The results demonstrate that LIBS detection technology combined IFFT and BP neural network is fast and accurate, which provides a new idea for batch detection of rice seeds.

**Document code:** A **Article ID:** 1673-1905(2022)08-0495-7

**DOI** <https://doi.org/10.1007/s11801-022-1137-3>

At present, the commonly used methods of rice identification are morphological identification, chemical identification, and molecular marker technology<sup>[1]</sup>, etc. But these methods have many limitations, such as low identification accuracy, complex and long identification process, high requirements for professional operation technology, which are not suitable for rapid batch detection and nondestructive analysis of rice seeds. In recent years, spectral technology has been widely used in rice detection. For example, LIN et al<sup>[2]</sup> used near infrared spectroscopy to identify transgenic Bt rice and its parents, and achieved good identification accuracy. SAMPAIO et al<sup>[3]</sup> used near infrared spectroscopy to effectively distinguish indica and japonica rice. WANG et al<sup>[4]</sup> fused the hyperspectral data of three rice varieties with the characteristics of chalkiness and rice shape, and established a discrimination model by reverse neural network with an accuracy of 94.45%. Moreover, LU et al<sup>[5]</sup> established a prediction model of rice seed moisture content based on hyperspectral technology combining clustering algorithm and support vector machine, which provided a reference for the quality monitoring and screening of rice seeds. ZHANG et al<sup>[6]</sup> established a classification model with good performance based on hyperspectral image technology for six groups of rice seed samples treated with different degrees of freezing injury.

Laser-induced breakdown spectroscopy (LIBS) is an element analysis method based on plasma emission spectroscopy<sup>[7]</sup>. Compared with other analytical methods,

LIBS technology requires no or less sample preparation and is non-destructive to sample. Besides, LIBS can simultaneously detect multiple elements in any form of sample, and has good adaptability to the environment. Due to its unique advantages, LIBS has been widely used in material classification and recognition in industry<sup>[8]</sup>, food<sup>[9,10]</sup>, geological exploration<sup>[11,12]</sup>, agriculture<sup>[13,14]</sup>, medicine<sup>[15,16]</sup>, etc. In view of the great potential of LIBS, an inverse fast Fourier transform (IFFT) method based on LIBS was proposed in this work to identify five common rice seeds in Hubei Province of China.

The experimental instrument used is RT100-HP LIBS. The laser source is a nanosecond Q-switched Nd:YAG 1 064 nm laser, meanwhile, it is equipped with a 670 nm red laser ablation point guiding laser to guide the user to select the ablation location. The laser ablation is uniform, ensuring efficient analysis of sample. The intensified charge coupled device (ICCD) detector and double-grating Cheney-Turner spectrometer are used to collect and analyze spectral signals. The TruLIBS emission spectrum database and powerful spectrum analysis tools are selected. In this experiment, the laser energy was 30 mJ, the laser spot size was 200  $\mu\text{m}$ , the gain intensity was 80, the detector sampling gate width was 3  $\mu\text{s}$ , the spectrum detection delay was 2  $\mu\text{s}$ , and the laser repetition frequency was 4 Hz. Five rice varieties used in the experiment were Luoyou 9348, Jingyou Xindao, Y Liangyou 302, Huayun Fudao and e Fufengyou 11, numbered from Sample 1 to Sample 5. There were 25 rice seeds of each variety, a

\* E-mail: 1924796334@qq.com

total of 125 samples. Every seed was measured 20 times at different positions. Due to the limited wavelength range of the optical signal collected by the ICCD detector each time, it is necessary to perform multiple segment measurements on the sample to obtain full spectrum. A total of 11 segmented spectra were collected, as shown in Tab.1, where *CWL* means the central wavelength of the spectrum.

**Tab.1 Wavelength range of sectional spectra**

| <i>CWL</i> (nm) | Wavelength range (nm) | Grating (mm) |
|-----------------|-----------------------|--------------|
| 250             | 222.176—275.783       | 2 400        |
| 290             | 263.623—314.187       | 2 400        |
| 330             | 305.156—353.411       | 2 400        |
| 370             | 346.488—390.207       | 2 400        |
| 405             | 383.109—423.478       | 2 400        |
| 440             | 420.188—455.561       | 2 400        |
| 490             | 432.146—541.897       | 1 200        |
| 570             | 515.755—619.844       | 1 200        |
| 650             | 598.747—696.388       | 1 200        |
| 730             | 682.758—772.428       | 1 200        |
| 810             | 765.379—848.525       | 1 200        |

There are obvious background noises in unprocessed spectra. These strong background noises affect the accuracy and stability of LIBS technology. Fig.1 shows the original spectrum and denoising spectrum. Take the three signal peaks with higher spectral intensity in Fig.1 as examples. Their signal-to-noise ratio (*SNR*) values are about 30.82 dB, 31.93 dB and 29.90 dB before denoising. After eliminating the background noise, their *SNR* values increase to 44.86 dB, 45.27 dB, and 40.43 dB, respectively. Obviously, compared with the original spectrum, the spectral *SNR* after eliminating the background noise is significantly improved.

Rice seeds are an organic matter, whose LIBS spectrum has atomic and ion spectrum lines, as well as molecular and molecular chain spectrum lines. Some spectrum lines will reduce the effect of type identification. Therefore, the spectral data need to be preprocessed. Fourier transform is a common tool in the field of signal processing, which can separate the signal from the interference and improve spectral *SNR*. However, the frequency-domain data obtained by Fourier transform is not integer. If it is forced to be converted into integer, it will cause data loss. Secondly, the spectral signal of rice seed is relatively complex, so its frequency-domain information is difficult to be represented by an image. Moreover, a frequency domain image can only reflect one frequency spectrum, and cannot simultaneously reflect the phase spectrum. Therefore, we consider the inverse fast Fourier transform (IFFT) to preprocess data. The time-domain signal can be obtained by IFFT, and its information contained is exactly the same as that contained in the original spectrum, only the expression of information different. The time-domain is less time-consuming

and simultaneously obtaining all the information of all frequencies. Based on above reasons, this paper uses the IFFT as the data preprocessing method.

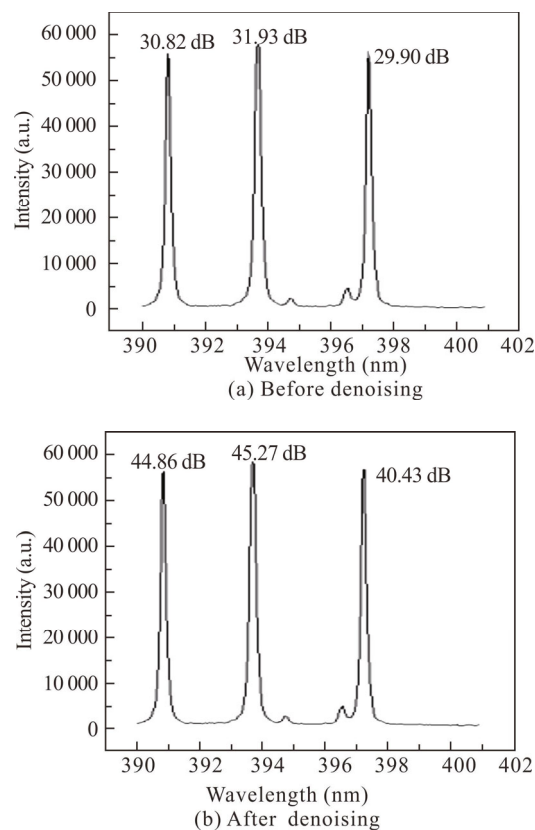


**Fig.1 Spectra of Sample 1**

The 11 segments of spectrum in Tab.1 were synthesized into a full spectrum with the wavelength range from 222.176 nm to 848.948 nm. Fig.2(a) illustrates the full spectrum of sample 1 at the 1st, 5th, 10th, 15th and 20th measurement, respectively. Due to the unstable laser energy output at the beginning, the spectrum of the first measurement is quite different from that of other sampling points. Though the spectra of other four sampling points are similar, there are still slight differences between them. This is because the element contents at different positions on the sample surface are not completely consistent, and the element content has a certain relationship with the spectral intensity, then the spectrum measured each time fluctuates slightly. Similarly, there are also slight differences in morphology and element content of different seeds of the same variety, so their spectra also have a certain difference. Fig.2(b) shows the spectra of five seeds in Sample 1. To reduce the error caused by the above factors, the spectra of 20 sampling points were identified, and the identification results were averaged. Overall, the spectra of five rice varieties, as shown in Fig.2(c), are extremely similar, which makes it impossible to intuitively distinguish sample spectra to classify the samples. Therefore, it is required to combine chemical metrology to achieve identification.

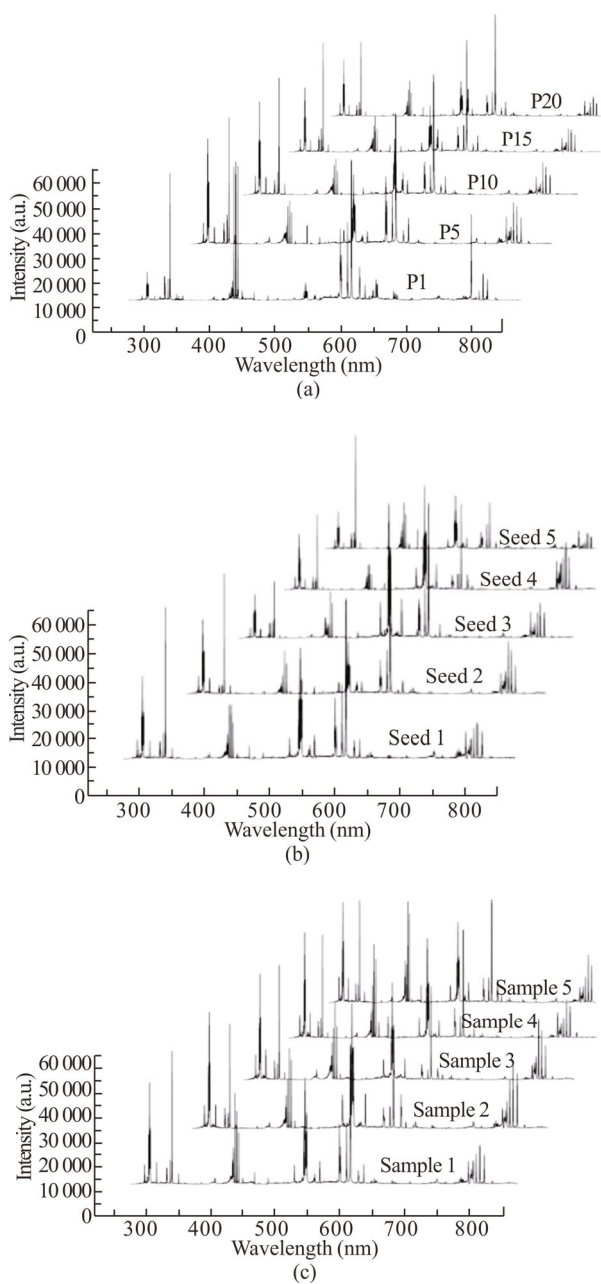


**Fig.2 Full spectra of samples: (a) Sample 1 at the 1st, 5th, 10th, 15th and 20th measurement; (b) Five seeds in Sample 1; (c) Five rice varieties**

Common chemical metrology methods include support vector machine (SVM), principal component analysis (PCA), back propagation (BP) neural network, etc. The sample data used in this work are large in scale, and SVM is difficult to implement for large-scale training samples. Besides, SVM is sensitive to parameter and kernel function selection. On the other hand, the time-domain signal intensity after IFFT has positive and negative value, which will result in unclear PCA comprehensive evaluation function and low naming clarity. The BP neural network has strong ability of nonlinear mapping, self-learning and adaptive, generalization and fault tolerance. So BP neural network is selected to es-

tablish the identification model. BP neural network refers to a multi-layer feedforward neural network trained by error BP algorithm. Its main framework consists of input layer, hidden layer and output layer, as shown in Fig.3.  $X_1, X_2, \dots, X_n$  are input signals,  $Y_1, Y_2, \dots, Y_m$  are output signals,  $W_{ij}$  and  $W_{jk}$  are connection weight matrix, and  $a_j$  and  $b_k$  represent weight bias. BP algorithm includes signal forward propagation and error back propagation. When propagating forward, the input signal acts on the output node through the hidden layer, and performs non-linear transformation layer-by-layer to generate the output signal. If the output signal is not the expected value, go to the back propagation of the error. The weights and thresholds of the network are iteratively adjusted according to the negative gradient descent direction, and the objective function is continuously trained to minimize the error. The weights and thresholds of BP neural network are randomly selected in the interval (0,1), and each weight bias is constant 1.

There are many factors that affect the performance of network evaluation, such as the complexity of network topology and the number of trainings. The complexity of topology mainly lies in the number of hidden layers and neurons. If the network is too simple, its performance will not meet the requirements. If the network is too complex, it will lead to huge computation and time consuming. The number of hidden layers, neurons, and training times, the learning speed and the target value of the performance function need to be determined according to the specific situation. The samples were divided into two groups, one was used for BP neural network training, and the other group was used for BP neural network testing. After testing multiple sets of neural network parameters, the BP neural network structure with one hidden layer was determined, and the numbers of neurons in the hidden layer and output layer were 30 and 5 respectively. The network training times was 5 000, the learning speed was 0.08, and the target value of the performance function was 0.001.

The identification rate of full spectrum before removing background noise is 86.14%, and that after denoising is 87.42%. The identification effect after denoising is slightly improved, so the data used in the subsequent analysis are with denoising. To further improve identification accuracy, the time-domain spectrum of the sample was used for identification. As shown in Fig.4(a), the time-domain spectrum after IFFT is symmetrically distributed. Therefore, to avoid the duplication of data and reduce the calculation amount of BP neural network, only the first 300, the first 500 and the first 1 000 data of the time-domain full spectrum were used for identification. The analysis results are listed in Tab.2, where  $IA$  represents the average identification accuracy of 20 measurement results,  $RSD$  represents the relative standard deviation of 20 measurement results, and  $IT$  represents the average identification time. When the first 500 data of the time-domain full-spectrum are used for type

identification, its identification accuracy is the highest, which is 95.28%. Compared with the full spectrum before IFFT, its identification accuracy increases by 7.86%, and the identification effect is greatly improved. When the first 300 data and the first 1 000 data of the time-domain full spectrum are used for identification, their identification effects are similar, and the identification accuracies are 92.16% and 92.63%, respectively. Obviously, for time-domain full spectrum, the best identification effect can be achieved when using only the first 500 data for type identification. Less than this data quantity, it will lead to lower identification accuracy due to less useful information. More than this data quantity, the recognition difficulty will be increased due to the similarity of too much data, and the improving effect will be weakened.

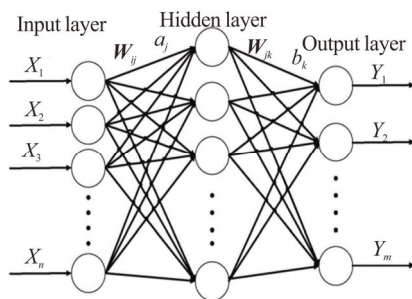


**Fig.3 BP neural network structure**

When the first 500 data of time-domain full spectrum are used for identification, the identification errors are mainly as follows. Sample 2 was classified as Sample 3 or Sample 3 was classified as Sample 2. These two types of errors account for approximately 84% of all errors. From Fig.2(c) and Fig.4(b), it can be seen that in both LIBS spectra and time-domain spectra, Sample 2 and Sample 3 are most similar. Meanwhile, the spectral differences between Sample 1, Sample 4 and Sample 5 increase after IFFT, while the spectral line difference between Sample 2 and Sample 3 becomes smaller and their spectral waveforms are more similar. Thus, it is prone to errors when identifying Sample 2 and Sample 3.

Though the identification accuracy of time-domain full spectrum is high, its identification time is too long. At the same time, since only one ICCD detector is installed in the RT100-HP spectrometer, it is necessary to synthesize segmented spectra to obtain full spectra, and the whole measurement process takes a long time. To solve above problems, segmented spectra were used for identification study. Tab.3 demonstrates the analysis results. It can be seen from Tab.3 that the identification accuracy of segmented spectra is quiet low, and the identification effects are extremely poor. The identification rates of only three segments of spectrum are above 70%, and the *CWLs* of these three spectra are 370 nm, 405 nm and 810 nm, respectively. Moreover, their *RSD* values are lower, indicating that their identification results have

higher stability and better reliability. Fig.5 shows that the spectra with the *CWLs* of 405 nm and 810 nm have higher *SNR*, so their identification accuracies are higher. The spectra with *CWLs* of 330 nm and 650 nm have lots of small-intensity signals and noises, and their *SNR* values are quite low. It is these noises and low-intensity signals that cause great interference to identification and weaken the identification effect.

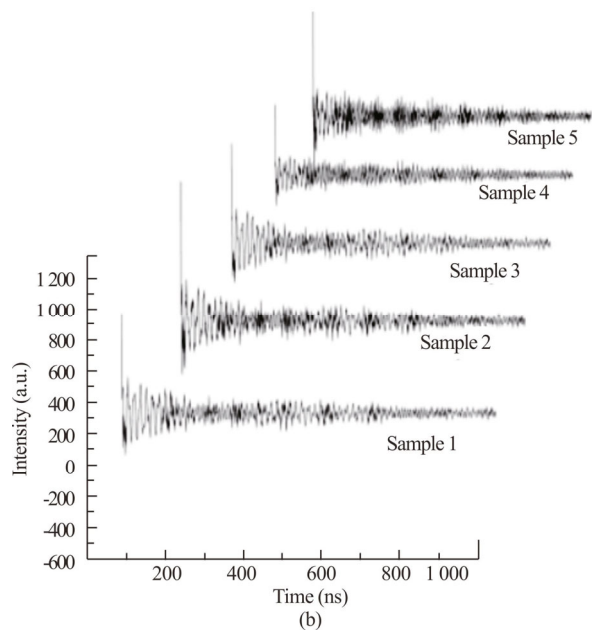
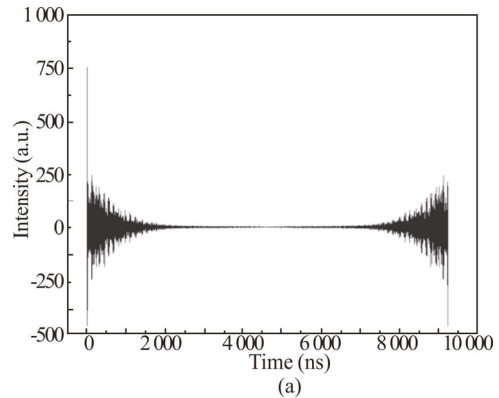


**Fig.4 Time-domain full spectra of (a) Sample 1 and (b) five samples**

**Tab.2 Identification results of time-domain full spectra**

| Data size            | <i>IA</i> (%) | <i>RSD</i> (%) | <i>IT</i> (s) |
|----------------------|---------------|----------------|---------------|
| The first 300 data   | 92.16         | 5.19           | 35.75         |
| The first 500 data   | 95.28         | 3.79           | 39.75         |
| The first 1 000 data | 92.63         | 3.20           | 31.94         |

Overall, the identification effects of segmented spectra are not ideal. The reason may be that the useful information contained in each segmented spectrum is not enough to distinguish the samples. Therefore, the three spectra

with the highest identification accuracy were combined for identification. Among the four groups of combined spectrum identification, the identification rates of combined spectra (370—405 nm and 370—810 nm) are not exceeding 80%, and these two combinations have little effect on improving identification effect. The identification rates of other two combined spectra (405—810 nm and 370—405—810 nm) exceed 80%, and these two combinations contribute to improving the identification effect. The identification rate of 370—405—810 nm combined spectrum is slightly lower than that of 405—810 nm combined spectrum, because the spectra with *CWLs* of 370 nm and 405 nm have overlapping parts of spectral lines, and the wavelength range of overlapping parts is from 383.109 nm to 390.207 nm. The overlapping part of the spectrum has a stronger peak, which has a greater impact on the identification. Consequently, when the spectra with *CWLs* of 370 nm and 405 nm are combined together to identify, the repetition of spectral information increases the difficulty of identification, and leads to a decrease in the identification accuracy on the contrary. Similarly, when a spectrum with *CWL* of 370 nm is added to the combined spectrum of 405—810 nm, its identification accuracy will also decrease.

**Tab.3 Identification results of segmented spectra**

| <i>CWL</i> (nm) | <i>IA</i> (%) | <i>RSD</i> (%) | <i>IT</i> (s) |
|-----------------|---------------|----------------|---------------|
| 250             | 56.30         | 16.92          | 3.98          |
| 290             | 65.42         | 10.04          | 3.67          |
| 330             | 49.66         | 7.68           | 2.46          |
| 370             | 72.92         | 6.95           | 5.87          |
| 405             | 75.72         | 5.71           | 5.40          |
| 440             | 57.68         | 11.49          | 3.49          |
| 490             | 64.14         | 6.33           | 3.06          |
| 570             | 68.76         | 5.82           | 2.50          |
| 650             | 43.58         | 10.71          | 2.17          |
| 730             | 60.56         | 10.10          | 4.19          |
| 810             | 73.44         | 6.50           | 3.16          |
| 370—405         | 77.10         | 4.69           | 7.72          |
| 370—810         | 78.26         | 5.13           | 6.15          |
| 405—810         | 82.10         | 5.18           | 7.02          |
| 370—405—810     | 81.74         | 5.44           | 4.29          |

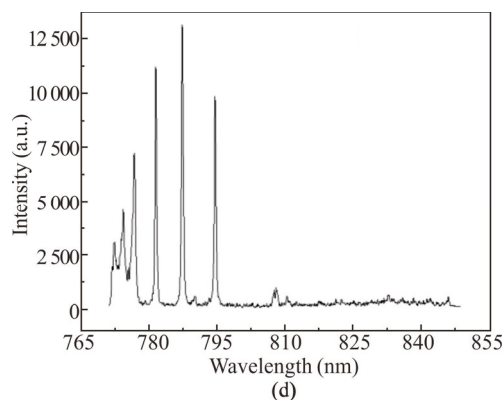
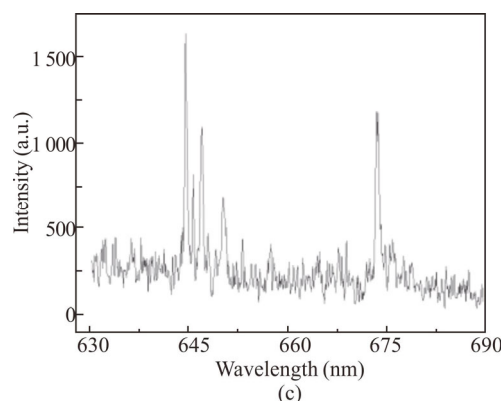
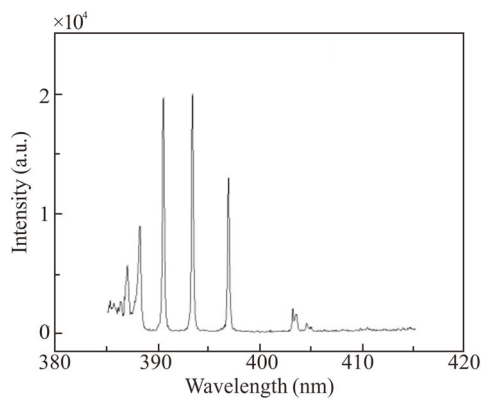
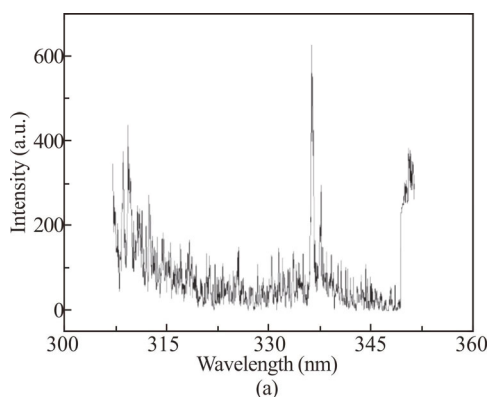


**Fig.5 Original segmented spectra with *CWLs* of (a) 330 nm, (b) 405 nm, (c) 650 nm and (d) 810 nm, respectively**

Next, the IFFT was performed on the segmented spectrum with the lowest identification rate (*CWL* of 650 nm), the three bands with the highest identification rate (*CWLs* of 370 nm, 405 nm and 810 nm) and the combined spectrum 405—810 nm. Then their time-domain signals were input into BP neural network for identification, and the analysis results are shown in Tab.4. Compared with the identification result before IFFT, the identification accuracy of the time-domain spectrum with *CWL* of 650 nm increases by 11.55 % at most. It means that the IFFT can also improve the identification effect for the band with low identification rate, but the improvement is limited. Moreover, the identification effect of the time-domain segmented spectrum with *CWL* of

405 nm is significantly improved as well. Nevertheless, the identification rate of the time-domain spectra with *CWLs* of 370 nm and 810 nm decreases instead of rising. Fig.6 shows the time-domain segmented spectra. It can be seen from Fig.6(b) that the time-domain spectrum with *CWL* of 405 nm still has a high *SNR*, and the spectral difference between samples also increases. So its identification effects are greatly improved when the time-domain spectral data with *CWL* of 405 nm are used for identification. While the signal intensity and *SNR* of the time-domain spectrum with *CWL* of 370 nm are quite low, as shown in Fig.6(a). Its spectral intensity undulates slightly before the 30th data, but the spectral intensity fluctuates around zero after the 30th data and the spectral line gets very gently, so there is almost no difference between the spectra of all samples. Likewise, for the time-domain spectrum with *CWL* of 810 nm, the difference between the other four samples is small except for Sample 3. And there is also almost no difference between the spectra of all samples after the 100th data. Therefore, although the time-domain spectrum with *CWL* of 810 nm has high *SNR*, its identification effect is also poor. The samples spectra with low *SNR* or high similarity will interfere with the identification and lead to low identification accuracy.

It can be found from Tab.4 that the identification accuracies of time-domain spectra increase first and then decrease with the increase of the data used. Taking the segmented spectrum with *CWL* of 405 nm as an example, when the first 100 data were used for identification, the identification rate was 91.44%, which was increased by 15.72% than that before IFFT. When the first 200 data were used for identification, the identification rate continued to increase to 94.36%. But when the first 300 data were used for identification, the identification rate decreased to 89.88%. Fig.6(b) shows that the spectral intensity is higher and fluctuates greatly before the 200 data, and there are great differences between the time domain spectra of the five samples. After the 200 data, the spectral intensity decreases to around zero, the spectral line tends to level off, and the difference between the spectra is greatly reduced. The other time-domain spectra also have similar cases. Because IFFT can be regarded as a band-pass filter, which filters a large number of useless interference information and retains useful spectral information, so that the useful information is separated from interference information. The spectral band with tiny intensity in the time-domain spectrum is the interference information. The more the interference information is, the worse the identification effect is. The effective information contained in the first 200 data of the time domain spectrum with a *CWL* of 405 nm is the most, so its identification accuracy is the highest, and the identification accuracy of the first 300 data is the lowest due to the increasing interference information.

**Tab.4 Identification results of time-domain segmented spectra**

| <i>CWL</i><br>(nm) | <i>IA</i> (%)         |                       |                       |
|--------------------|-----------------------|-----------------------|-----------------------|
|                    | The first<br>100 data | The first<br>200 data | The first<br>300 data |
| 650                | 55.13                 | 53.27                 | 47.48                 |
| 370                | 69.63                 | 63.85                 | 56.33                 |
| 405                | 91.44                 | 94.36                 | 89.88                 |
| 810                | 76.26                 | 62.66                 | 45.74                 |
| 405—810            | -                     | 92.10                 | 94.40                 |

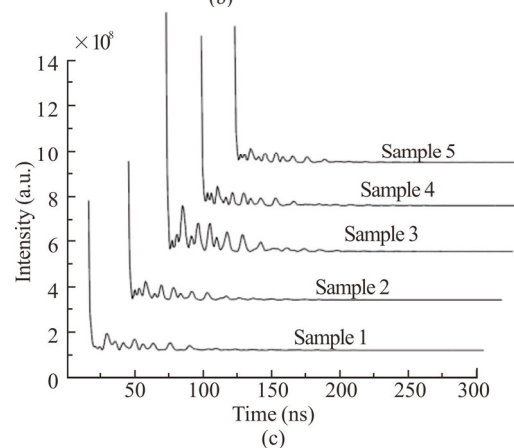
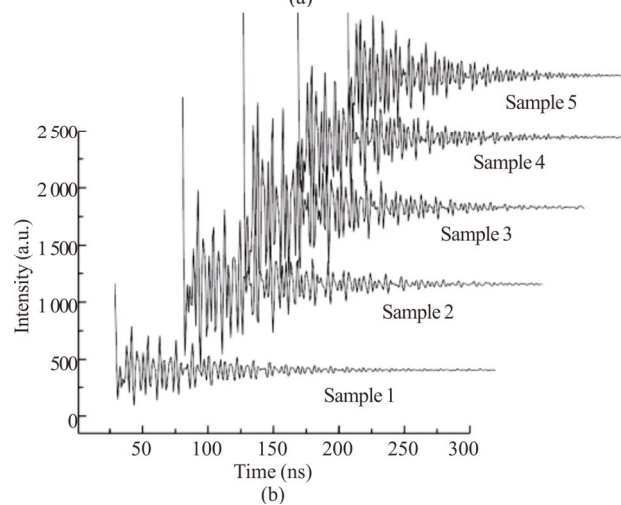
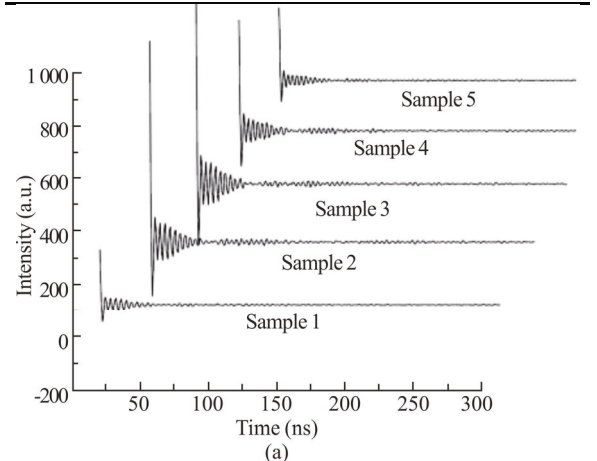


**Fig.6 Time-domain segmented spectra with *CWLs* of (a) 370 nm, (b) 405 nm, and (c) 810 nm, respectively**

The spectral intensity of the combined spectrum 405—810 nm in time domain tends to zero after the 300th data, and the spectral band after the 300th data is unfavorable for type distinction of samples. On the other hand, the useful information contained in the first 100 data is too little for the combined spectrum, so it would be difficult to achieve the purpose of improving identification effect. Therefore, only the first 200 data and the first 300 data of time-domain combined spectrum were used for identification analysis. When the first 200 data were used for identification, the identification accuracy was 92.10%, while when the first 300 data were used for identification, the identification accuracy was 94.40%. The identification effects of the time-domain combined spectrum are similar to those of the time-domain segmented spectrum with a *CWL* of 405 nm, and their identification time is shorter, all within 10 s. It demonstrates that the segmented spectrum with a *CWL* of 405 nm plays a major role in identification of time-domain combined spectrum, while the spectrum with *CWL* of 810 nm has little effect on the combined spectrum identification.

The IFFT method based on LIBS has achieved good classification results for the identification of full spectrum, segmented spectrum with *CWL* of 405 nm and combined spectrum of 405—810 nm, and their identification accuracies are above 94%. The identification effect of time-domain full spectrum is the best, but its measurement time and identification time are very long, which is not suitable for fast identification. The identification time of time-domain segmented spectrum and combined spectrum is very short, which is more suitable for rapid batch detection of rice seeds. The combination of IFFT and piecewise modeling greatly reduces the data dimension of LIBS, and improves the identification accuracy as well as speed. In future research, varieties of rice samples will be increased to further study the universality of LIBS for rice identification, and further improve the identification accuracy and the stability of the identification results at the same time.

### Statements and Declarations

The authors declare that there are no conflicts of interest related to this article.

### References

- [1] YU S J. Identification methods and application status of rice varieties purity[J]. Heilongjiang agricultural sciences, 2015, (8): 145-148. (in Chinese)
- [2] LIN P, GAO M Q, CHEN Y M. Rapid identification method of Bt transgenic rice seeds and their parents based on near infrared spectroscopy analysis technology[J]. Jiangsu agricultural sciences, 2019, 47(13): 72-75. (in Chinese)
- [3] SAMPAIO P S, CANSTANHO A, ALMEIDA A S, et al. Identification of rice four types with near-infrared spectroscopy associated with PLS-DA and SVM methods[J]. European food research and technology, 2020, 246(3): 527-537.
- [4] WANG L, LIU D, PU H, et al. Use of hyperspectral imaging to discriminate the variety and quality of rice[J]. Food analytical methods, 2015, 8(2): 515-523.
- [5] LU B, SUN J, YANG N, et al. Hyperspectral detection for moisture in rice seeds by SAGA-SVR prediction model[J]. Journal of southern agriculture, 2018, 49(11): 2342-2348. (in Chinese)
- [6] ZHANG L, SUN H, RAO Z H, et al. Hyperspectral imaging technology combined with deep forest model to identify frost-damaged rice seeds[J]. Spectrochimica acta part A: molecular and biomolecular spectroscopy, 2020, 229: 117973.
- [7] SHAH S K H, IQBAL J, AHMAD P, et al. Laser induced breakdown spectroscopy methods and applications: a comprehensive review[J]. Radiation physics and chemistry, 2020, 170: 108666.
- [8] SUNGHO S, YOUNGMIN M, JAEPIL L E E, et al. Improvement in classification accuracy of stainless steel alloys by laser-induced breakdown spectroscopy based on elemental intensity ratio analysis[J]. Plasma science and technology, 2020, 22(7): 074011.
- [9] STEFAS D, GYFTOKOSTAS N, COURIS S. Laser induced breakdown spectroscopy for elemental analysis and discrimination of honey samples[J]. Spectrochimica acta part B: atomic spectroscopy, 2020, 172: 105969.
- [10] VELIOGLU H M, SEZER B, BILGE G, et al. Identification of offal adulteration in beef by laser induced breakdown spectroscopy (LIBS)[J]. Meat science, 2018, 138: 28-33.
- [11] KUMAR N, LAN Y, LU Y, et al. Development of a micro-joule portable LIBS system and the preliminary results for mineral recognition[J]. Optoelectronics letters, 2018, 14(6): 401-404.
- [12] CHEN X L, DONG F Z, TAO G Q, et al. Application of laser-induced breakdown spectroscopy in rapid identification of geological logging lithology[J]. China laser, 2013, 40(12): 1215001.
- [13] PÉREZ-RODRÍGUEZ M, DIRCHWOLF P M, SILVA T V, et al. Fast spark discharge-laser-induced breakdown spectroscopy method for rice botanic origin determination[J]. Food chemistry, 2020, 331: 127051.
- [14] MARTINO L J, D'ANGELO C A, MARINELLI C, et al. Identification and detection of pesticide in chard samples by laser-induced breakdown spectroscopy using chemometric methods[J]. Spectrochimica acta part B: atomic spectroscopy, 2021, 177: 106031.
- [15] GAUDIUSO R, EWUSI-ANNAN E, XIA W, et al. Diagnosis of Alzheimer's disease using laser-induced breakdown spectroscopy and machine learning[J]. Spectrochimica acta part B: atomic spectroscopy, 2020, 171: 105931.
- [16] TENG G, WANG Q, ZHANG H, et al. Discrimination of infiltrative glioma boundary based on laser-induced breakdown spectroscopy[J]. Spectrochimica acta part B: atomic spectroscopy, 2020, 165: 105787.